New ELF Observation System at Moshiri, Japan and Assessments of Acquired Data

Yoshiaki Ando[(1)], Pavlo Maltsev[(2)], Andriy Sukhynyuk[(2)], Takeyoshi Goto[(1)], Takeshi Yamauchi[(1)], Yasuhide Hobara[(3)], Minako Sekiguchi[(1)], Yuji Ikegami[(4)], Masayuki Sera[(4)], Varely Korepanov[(2)], and Masashi Hayakawa[(1)]

(1) Department of Electronic Engineering, The University of Electro-Communications, Tokyo, Japan
(2) L'viv Centre of Institute of Space Research, National Academy of Sciences and National Space Agency of Ukraine, L'viv, Ukraine
(3) Swedish Institute of Space Physics, Kiruna, Sweden
(4) Solar-Terrestrial Environment Laboratory, Nagoya University, Nagoya, Japan

Abstract. This paper describes the installation of a new observation system to measure magnetic fields in extremely low frequency band at Moshiri, Hokkaido, Japan. Then, we perform assessment of data acquired by the new system. The results show that the installation was successful and that Moshiri is very appropriate for the observation because of the satisfactory electromagnetic environment, i.e. low human noise. A signal processing is given for the estimation of Schumann resonance spectra to demonstrate the advantage of the new system. By this processing, the Schumann resonances clearly appear even in the time when local lightnings are active.

Key words: ELF observation, search-coil magnetometer, Schumann resonance

1 Introduction

This paper reports the installation of a new observation system to measure magnetic fields in extremely low frequency (ELF) band at Moshiri, Hokkaido, Japan, in July 2004. We perform assessment of data acquired by the new system. And a signal processing is given for the estimation of the Schumann resonance spectra to demonstrate the advantage of the new system.

The study of ELF electromagnetic fields is of essential importance from the viewpoint of natural electromagnetic phenomena, e.g. lightnings and earthquakes[*Nickolaenko and Hayakawa*, 2002; *Hayakawa*, 1999]. Especially, the report on the global thermometer by using Schumann resonances have made an intense impact on the ELF study[*Williams*, 1992]. Also, the findings of photoluminescent phenomena in the mesosphere and the lower ionosphere, so-called Sprites and Elves, motivate researchers in this field to use the ELF band as a radiometer of lightnings to excite them[*Huang et al.*, 1999]

From those necessities, we started the ELF electromagnetic field measurement at Moshiri(44° 20′N 142° 15′E), Hokkaido, Japan since 1999[*Hobara et al.*, 2000], and have made continuous wide-band measurements. The results have been providing significant information on the atmospheric electromagnetics[*Hobara et al.*, 1999]. The study of ELF, nevertheless, remains important with the development of the surrounding researches.

In 2004 we renewed the experimental system to include recent technologies into collection of data and to improve the quality of measurement. Especially, the development of personal computers and the increase of storage capacity permit us to acquire continuous waveform with enough high sampling rate within good precision. Moreover, storing the waveform enables us to perform various signal processings to the data.

In this paper, we describe the schematics of the new system, assess the collected data, and show an example of the signal processing specialized for the study on Schumann resonances.

2 The observation system

The system is designed and produced by L'viv Centre of Institute of Space Research, National Academy of Sciences and National Space Agency of Ukraine. The present system consists of two magnetometers, a global positioning system (GPS) for time synchronization, a PC with a data acquisition board (DAQ), and the terminal box. In this section, we provide the schematic description on the system.

2.1 Magnetometer LEMI-116

The LEMI-116 is a search-coil magnetometer with a magnetic core (see Fig. 2). The length is 1215 mm, the diameter is 96mm, and the weight is about 8 kg. The three lots in Fig. 2 were designed to measure magnetic fields in the frequency range 0.1 Hz to 1 kHz. The frequency characteristics is adapted to be linear at < 1 Hz, and flat from 1 Hz- by internal pre-amplifiers, and set to 20 mV/nT output in flat range as shown in Fig.1. Moreover, the auxiliary output of 200 mV/nT is also prepared. The measurement noise is quite low and smaller than 10 pT/$\sqrt{\text{Hz}}$, 0.2 pT/$\sqrt{\text{Hz}}$, 0.01 pT/$\sqrt{\text{Hz}}$, and 0.003 pT/$\sqrt{\text{Hz}}$ at 0.1 Hz, 1.0 Hz, 10 Hz, and 100 Hz, respectively. Perfect waterproof is realized in the magnetometers. A low-pass filter is built inside to avoid aliasing effects in the discrete Fourier transform[*Press et al.*, 1992], and the cut-off frequency is 1.3 kHz. The magnetometer outputs signals in differential-mode, and is transfered in a shielded twisted pair (STP) cable (5-pairs including power supply to amplifiers).

2.2 Data acquisition

The signal transmitted through the STP cables is fed directly into the data acquisition board (National Instruments PCI-MIO-16XE-50) and amplified by the internal amplifiers. The time synchronization is realized by using GPS (Trimble Lassen SK-II), and the communication with the GPS module is made in Trimble Standard Interface Protocol (TSIP) through the serial-port of PC. The sampling frequency for storing data is flexible by the acquisition software and ranges 1 Hz up to 4 kHz. The 4 kHz-sampled data are collected and the down-sampling is performed for storing by averaging collected data. Currently, the 4 kHz data are begin stored.

2.3 Installation on the site

We chose Moshiri (44° 20′N 142° 15′E), Hokkaido, Japan as our observation site because Moshiri is located in a rural area and it is available to use an observatory building with cooperation of the Solar-Terrestrial Environment Laboratory of Nagoya University.

The magnetometers are installed at the distance of 180 m, approximately, from the building where the system for data acquisition is put. The magnetometers and the DAQ system are connected by about 220 m-cables. The GPS antenna for time synchronization is put on the top of a pole with the height of 6 m which is located just outside the building.

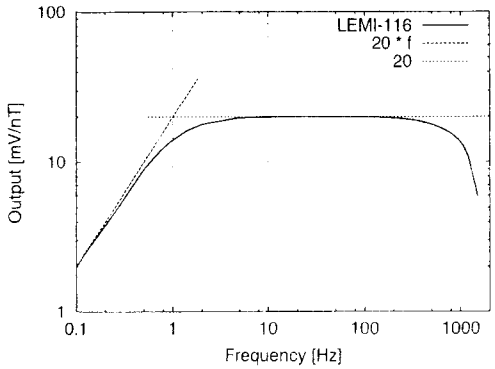

Figure 1: Frequency characteristics of LEMI-116 output.

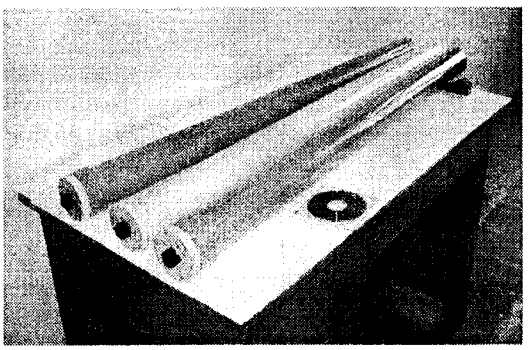

Figure 2: Photograph of the magnetometer LEMI-116 (three lots).

Two magnetometers are buried under the ground at the depth of about 50 cm, and are directed to the geomagnetical north and the east, where the directions were determined by a simple compass, and a few degrees of the error are possible. From the magnetometers, the cables run under the ground along about 40 m-distance, and then come up over the ground. The remains of the cables were fixed by poles which stand at every 10 m-distance and by the wire to connect the poles, and run in the air at the height of 3-4 m to the building. Note that the cables have no junctions except for the both ends.

The magnetometers were calibrated to measure the frequency characteristics at the production stage. We therefore made an easy check at the field site to investigate damages in transportation. Two magnetometers are fixed with opposite directions to each other, and the sum of two responses is measured. We brought one more magnetometer and the cross-checking among them was performed. It was examined that the summed signal decreased drastically to zero-level, and that no particular frequency dependence appeared.

3 Assessment and processing of acquired data

3.1 Assessment of acquired data and electromagnetic environment of the site

Fig.3 shows the time series of sampled data collected by the new system described in the previous section. The data were collected on 15th July 2004, and the ones from 16:34:17UT to 16:34:23UT are plotted. The horizontal axes stand for the time past 16:34:17UT. The dominant part of data is 50 Hz and the harmonic signals radiated from the commercial power supply system, and the magnitudes are about 0.07 and 0.23 nT peak to peak in the north-south and the east-west components, respectively, and it is considered to be due to the local configuration of the power system. These values are extremely small in comparison with other areas in Japan. In the urban area like Tokyo, Japan, the 50 Hz and the harmonic noise has the magnitude of several ten nano-Tesla, and we examined that it is about 40 nT at the suburban city, Chofu in Tokyo. Even in the anechoic chamber of the University of Electro-Communications, the magnitude decreases down to about 4 nT because the chamber is not designed to be effective at such low frequencies. Consequently, Moshiri in Hokkaido, Japan, is one of the best area to measure the ELF fields considering the availability of stable electricity and the observation building where the acquisition system is put.

It is observed at about 4.77 sec in Fig. 3(c) that the impulse signal is detected and they are generated by the lightnings near the observation site.

3.2 Estimation of spectrum density of Schumann Resonances

The biggest advantage of the present system is that we can process collected data according to our purposes. For example, we can insert any kinds of filters, even acausal (noncausal) ones, into the same data separately. In this paper, we demonstrate an estimation of the spectrum density of Schumann resonances (SR). Especially, our attention is put on the frequency range up to 50 Hz, and also on long-term variance of the spectra on the order of ten minutes.

A consideration is necessary for the spectrum density estimation in the present case because there are special frequencies where the spectrum curve show extraordinary peaks, i.e. radiation from commercial power supply systems as mentioned earlier. The frequency of the power supply at our field site is 50Hz, and the higher harmonic frequencies are also observed. The spectra of the radiation is quite narrow, but not ideally discrete. This fact indicates that it is significant to consider the data windowing for the discrete Fourier transform (DFT) to reduce the influence from neighbor frequencies. In the present analyses we use the Hann window given by

$$W_j = \frac{1}{2}\left[1 - \cos\left(\frac{2\pi j}{N}\right)\right], \quad j = 1, 2, \cdots, N, \tag{1}$$

where N is the number of sampled data to be transformed. This choice is reasonable because the spectrum of Hann window decreases rapidly apart from zero frequency, and the estimated value at a frequency is not influenced from the values far from the frequency.

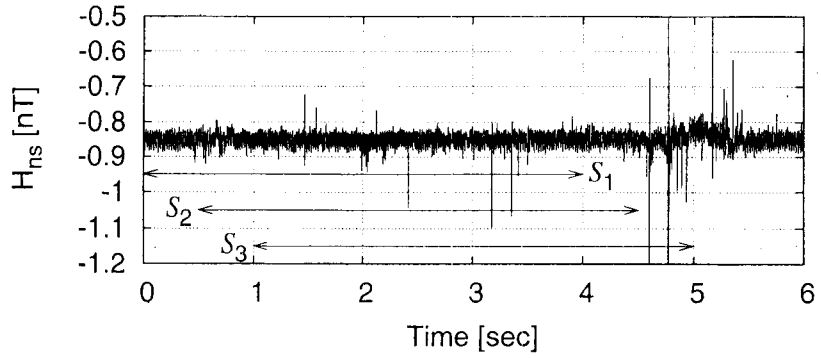

(a) The north-south component. The embedded symbols, S_1, S_2, and S_3 are used in Sec.3.2

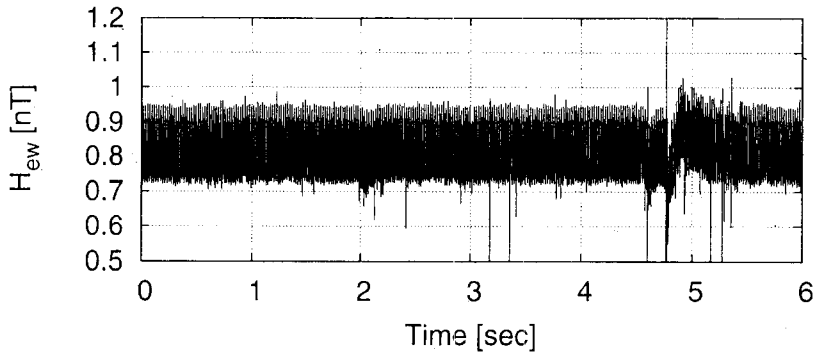

(b) The east-west component.

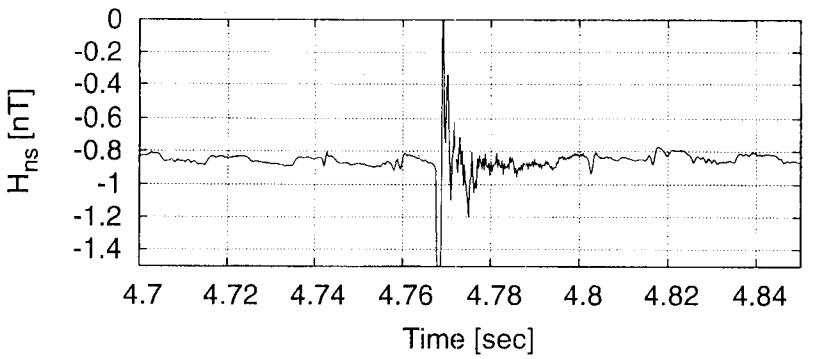

(c) The enlarged figure around 4.77 sec

Figure 3: The magnetic field measured by the new system. Note that the biased component is meaningless. The time in the horizontal axis is measured from 16:34:17UT on 15th July, 2004. The lowest panel is the one to enlarge the period when an impulse was detected. The magnitude of the impulse at about 4.77 sec is 6 nT peak to peak.

It is significant in estimating the SR spectra to consider one more thing which is the existence of impulse signals generated by lightning strokes in the vicinity of the observation point. A typical example in actually measured data was already shown in Fig. 3. Note that the intense pulse is observed at about 4.77 sec as depicted in Fig. 3(c). These transient signals make it difficult to estimate the SR spectra precisely just only by DFT because the SR, a stationary phenomenon, has smaller intensity and is easily hidden by the spectra of such impulses. In order to demonstrate the above statement, we take three sets of data from Fig. 3(a), $\mathcal{S}_1$, $\mathcal{S}_2$, and $\mathcal{S}_3$, collected from 0.0 sec to 4.0 sec, from 0.5 sec to 4.5 sec, and from 1.0 sec to 5.0 sec, respectively. The three sets have equal number of points, and the actual time periods are the same, i.e. 4 sec. Fig. 4 shows the three spectra of the north-south component obtained by taking the DFT of $\mathcal{S}_1$, $\mathcal{S}_2$, and $\mathcal{S}_3$. It is clearly understood that the two spectra, $\mathcal{S}_1$, and $\mathcal{S}_2$, are very similar, which is demanded in the SR investigation because SRs do not vary so rapidly. The spectrum obtained from $\mathcal{S}_3$, however, is very different from the others, and the reason is apparently the existence of the impulse. We can conclude that it is necessary to process the data to remove such affection for better estimation of SR spectra.

The one of good estimation is to remove the impulse signals by using the linear prediction[*Haykin*, 1996]. The resultant waveform and the spectra are given in Figs. 5 and 6. It is observed that the impulse signals are removed and the spectra are not so influenced by fractional difference in time of data.

The linear prediction is used to extrapolate future data, $a_{N+1}, a_{N+2}, \cdots$, by means of the autocorrelation of the past data, $a_1, a_2, \cdots, a_N$ under the assumption of stationarity, and the predicted value, a_{N+1} is given as a kind of filters by

$$a_{N+1} = \sum_{j=1}^{M} d_j a_{N+1-j}, \tag{2}$$

where d_j's are the filter coefficients. By using the predicted value, a_{N+1}, we can derive the next prediction, a_{N+2}, and the recursive prediction allows us to extrapolate the data from $N+1$ to $N+K$ provided that the stability of the filter is satisfied. The coefficients are derived as follows: if we have a sequence of sampled data, $a_1, a_2, \cdots, a_N$, the autocorrelation ϕ_j is given by

$$\phi_j = \frac{1}{N-j} \sum_{i=1}^{N-j} a_i a_{i+j}. \tag{3}$$

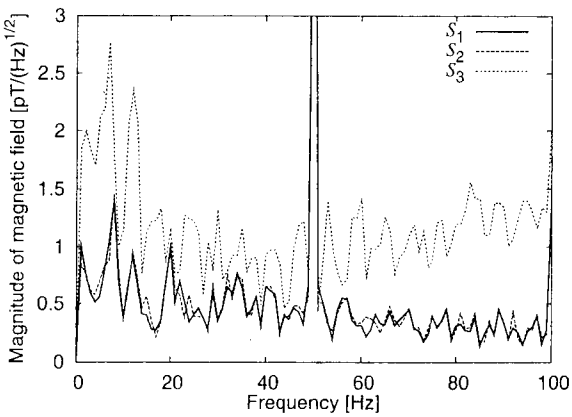

Figure 4: Three spectra obtained from $\mathcal{S}_1$, $\mathcal{S}_2$, and $\mathcal{S}_3$.

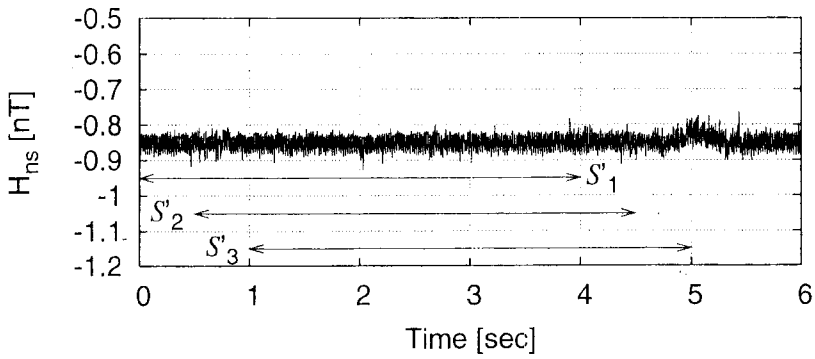

(a)

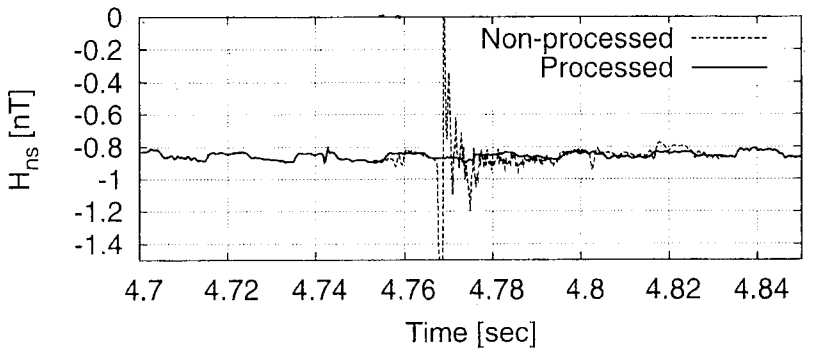

(b)

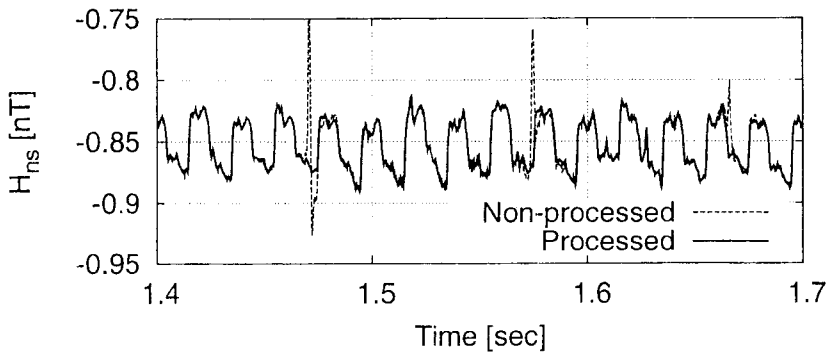

(c)

Figure 5: Processed waveforms and spectra by the linear prediction. Non-processed ones are also plotted as a reference.

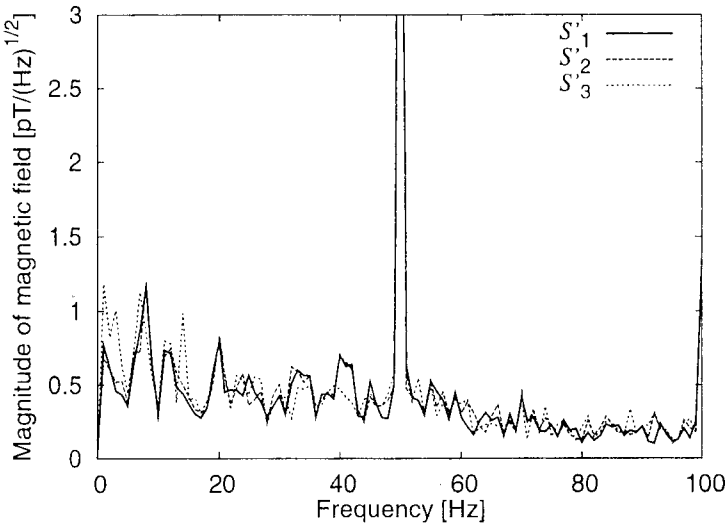

Figure 6: The spectra obtained from the processed data by the linear prediction.

Then, the coefficients for the linear prediction are obtained by solving the linear equation:

$$\begin{bmatrix} \phi_0 & \phi_1 & \cdots & \phi_{M-1} \\ \phi_{-1} & \phi_0 & \cdots & \phi_{M-2} \\ \vdots & \vdots & & \vdots \\ \phi_{1-M} & \phi_{2-M} & \cdots & \phi_0 \end{bmatrix} \cdot \begin{bmatrix} d_1 \\ d_2 \\ \vdots \\ d_M \end{bmatrix} = \begin{bmatrix} \phi_1 \\ \phi_2 \\ \vdots \\ \phi_M \end{bmatrix} \tag{4}$$

Note that $\phi_{-j} = \phi_j$. The stability is satisfied if and only if the roots of the characteristic equation in the Z-transformed domain

$$z^M - \sum_{j=1}^{M} d_j z^{M-j} = 0 \tag{5}$$

exist in the unit circle $|z| \leqq 1$. For the case that the coefficients found is unstable, there are some manipulation for the stability[Press et al., 1992], but it is not necessary if the predicted period is as quite short as the present case. We apply the above method to the data detected as impulse signals.

The detection of impulses and the application of the linear prediction are as follows:

1. A segment of sequential data is picked up, and if the previous segment was processed, the small part at the end of the previous segment is overlapped as the beginning of the segment to be processed.

2. Ideal filtering: we take the DFT of the segment to get the spectrum, and set the values be zero in the following frequency ranges:

   (a) an ideal band eliminating filter: $50n - 2 \leqq f \leqq 50n + 2, \quad (n = 1, 2, \cdots)$

   (b) an ideal high-pass filter: $0 \leqq f \leqq \xi_l$.

   These filters are intended to eliminate the radiation from power supply systems, and to eliminate long-term variation. Then, the resultant spectrum is transformed into the time series data by the inverse DFT.

3. The linear prediction is applied to the ORIGINAL data (not the one through the above filters) in the region where the ideal-filtered data exceed a criterion, η_l, i.e. this region is regarded as an impulse. The regions of the original data are replaced with the predicted data, and the result is set as the original data for the next, the $(l+1)$th step.

4. The ideal filtering and the linear prediction are repeated L times with increase of the cut-off frequency, ξ_l, and with decrease of the criteria, η_l.

5. repeat the above procedures until the entire data are processed.

In the present analyses, ξ_l and η_l are chosen as follows:

$$\xi_l = \frac{l}{L}(\xi_L - \xi_0) + \xi_0 \quad [\mathrm{Hz}], \tag{6}$$

$$\eta_l = (\eta_0 - \eta_L)\frac{e^{-l/5} - e^{-5}}{1 - e^{-5}} + \eta_L \quad [\mathrm{nT}], \tag{7}$$

i.e. the cut-off frequency of the ideal filter increases linearly from ξ_0 to ξ_L, and the criterion for the detection of impulses decreases exponentially from η_0 to η_L.

The parameters used are : $N = 4000$, i.e. 1 sec, $M = 640$, $K = 80$, $L = 25$, ξ_0=10 Hz, ξ_{25}=50 Hz, η_{25}= 0.03 nT, and η_0 is the maximum value of the time-series data after the first ideal filtering. N and M are chosen by a numerical experiment.

Fig. 7 shows the daily variation of the SR spectra obtained from the north-south component with the above-mentioned processing as a colormap. The data were collected on 15 August 2004. The spectra are calculated every ten minutes, and each spectrum is averaged from 120 spectra obtained from 10 seconds data and the first half of them, i.e. 5 seconds data, is overlapped on the second half of another 10 seconds data. As a reference, the corresponding non-processed spectra are shown in Fig.8. Note that the horizontal axis in the figures is written in the universal time (UT), and the conversion from the UT to the local time (LT) is plus nine hours. It is seen that in the diurnal time the magnitude of the spectra is strong while they have small values in the nocturnal time. We can interpret this fact as caused by lightnings near the observation site, and not by global lightning activity, because lightning is more active in the diurnal time generally[*Nickolaenko*, 2002].

Fig. 9 shows the spectra at a particular time, and Fig. 9(a) is the ones at 18:00UT (03:00LT on 16th, August) when the local lightning activity is low. We can observe that the non-processed spectrum has higher noise floor because of the impulses. On the other hand, Fig. 9(b) depicts the ones at 06:00UT (15:00LT). Two spectra are very different from each other. The SR peaks are hidden in the non-processed spectrum which is drastically disturbed by the impulses. The processed spectrum still has the clear peaks, and the improvement by the present method is prominent.

Additionally, it is extremely surprising that the 60 Hz noise from another power supply systems becomes visible in the processed spectra as pointed by the arrow in Fig.9(b). This small peak can be observed all over the day, and it is rarely found even in non-processed spectra. To our best knowledge, there are no cause to excite such a discrete 60 Hz spectrum over whole a day in the vicinity of the observation site. One of the most possible source is the power system in the western Japan where the systems work at 60 Hz. The harmonics of 60 Hz are not observed, and it is considered that the losses of propagation and conduction is larger at the higher frequencies. Of course, without the processing the 60 Hz noise is not as outstanding. We can conclude that such a careful processing to extract small signals is accomplished by measuring with the use of the low-noise magnetometer, LEMI-116, and storing all sampled data without preliminary processings.

4 Conclusion

We have described the observation system to measure the ELF magnetic fields, and the installation process at the field site, Moshiri. The installation was successful and the data have been being collected

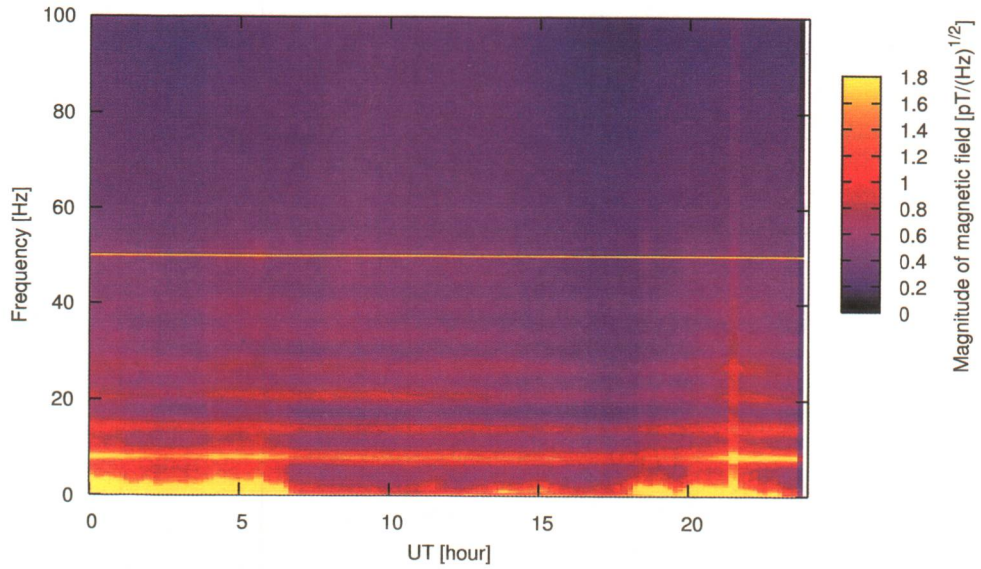

Figure 7: The daily variation of the averaged spectra processed by the linear prediction.

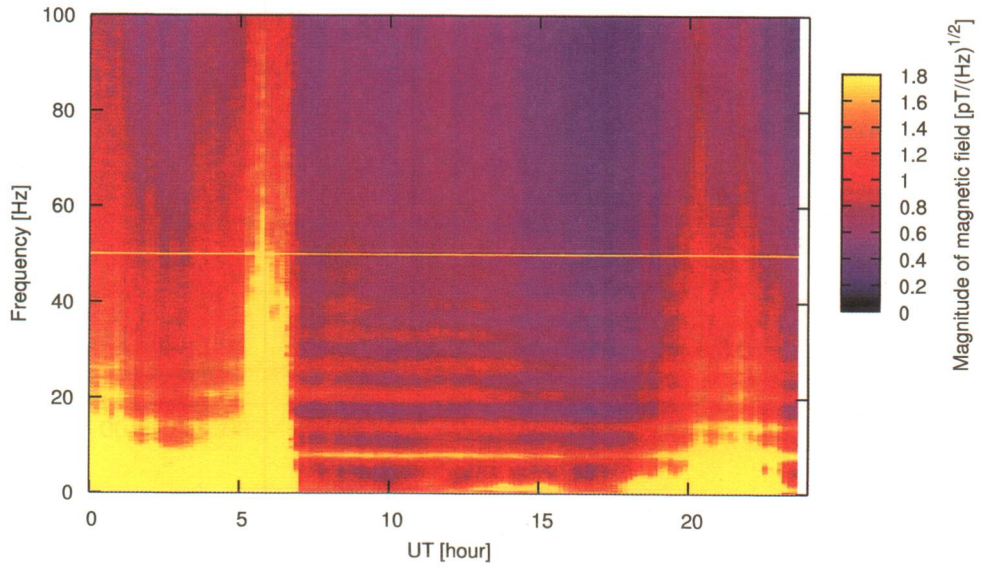

Figure 8: The daily variation of the averaged spectra directly calculated from the original data.

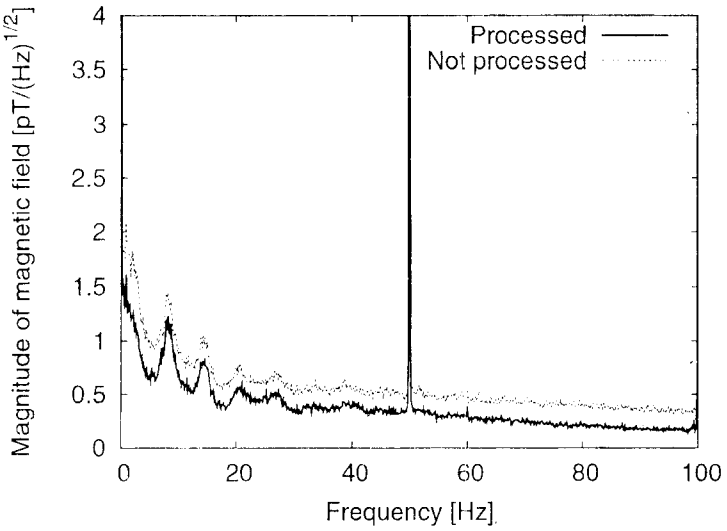

(a) 18:00UT 15th August 2004

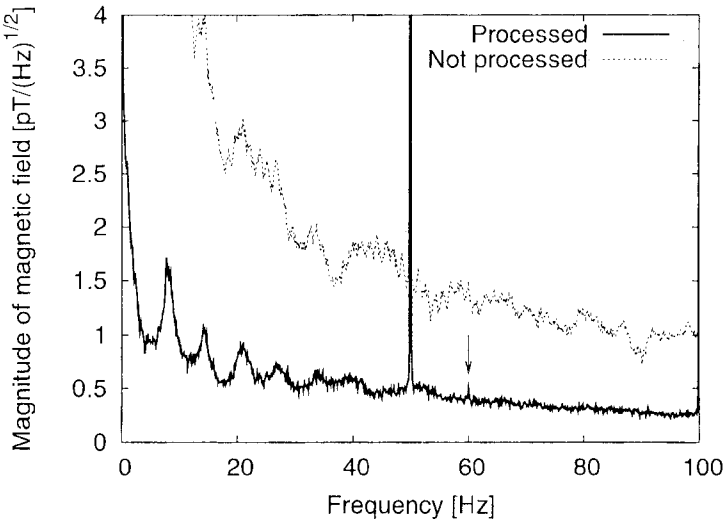

(b) 06:00UT 15th August 2004

Figure 9: Particular spectra averaged over 10 minutes with and without the linear prediction.

since July 2004. The dominant component of signals is the noise from power supply systems, and the magnitudes are about 0.07 and 0.23 nT peak to peak in the north-south and the east-west components, respectively, and the result indicates that the chosen site is very appropriate for observation because of the small human noise.

An example of signal processing has been given for the estimation of Schumann resonances by means of the linear prediction. The processed data show the global resonant peaks clearly without the disturbance of local impulse signals. We conclude that these successful results can be achieved by the new observation system to store complete waveforms with good precision and high sampling.

Acknowledgments

This study is granted by the young scientists support of the Department of Electronic Engineering, The University of Electro-Communications.

References

M. Hayakawa, Editor, *Atmospheric and Ionospheric Electromagnetic Phenomena Associated with Earthquakes*, TERRAPUB, Tokyo, Japan, 1999.

S. Haykin, *Adaptive Filter Theory*, Prentice-Hall, Upper Saddle River, NJ, 3rd edition, 1996.

Y. Hobara, N. Iwasaki, T. Hayashida, M. Hayakawa, K. Ohta, and H. Fukunishi. Interrelation between ELF transients and ionospheric disturbances in association with Sprites and Elves, *Geophys. Res. Lett.*, 28(5):935–938, 2001.

Y. Hobara, N. Iwasaki, T. Hayashida, N. Tsuchiya, E. R. Williams, M. Sera, Y. Ikegami, and M. Hayakawa. New ELF observation site in Moshiri, Hokkaido Japan and the results of preliminary data analysis. *J. Atmos. Electr.*, 20(2):99–109, 2000.

E. Huang, E. Williams, R. Boldi, S. Heckman, W. Lyons, M. Taylor, T. Nelson, and C. Wong, Criteria for sprites and elves based on Schumann resonance observations, *J. Geophys. Res.*, 104(D14):16,943–16,964, JULY 1999.

A. P. Nickolaenko and M. Hayakawa, *Resonances in the Earth-Ionosphere Cavity*, Kluwer, Dordrecht, Netherlands, 2002.

W. H. Press, S. A. Teukolsky, W. T. Vetterling, and B. P. Flannery, *Numrical Necipes*, Cambridge University Press, Cambridge, 2nd edition, 1992.

E. R. Williams, The Schumann resonance: a global tropical thermometer, *Science*, 256:1184–1187, 1992.

(Received January 14, 2005; revised February 17, 2005; accepted February 25, 2005)